Research Article Vol. 56, No. 17 / June 10 2017 / Applied Optics 4961

applied optics

Optical design and fabrication of palm/fingerprint uniform illumination system with a high-power near-infrared light-emitting diode

Lei Jing,[1,*] Yao Wang,[1] Huifu Zhao,[2] Hongliang Ke,[1,3] Xiaoxun Wang,[1,3] and Qun Gao[1]

[1]Changchun Institute of Optics, Fine Mechanics and Physics, Chinese Academy of Sciences, No. 3888, East South-Lake Road, Changchun, Jilin 130033, China
[2]School of Electro-Optical Engineering, Changchun University of Science and Technology, No. 7089, Wei-xing Road, Changchun, Jilin 130022, China
[3]University of Chinese Academy of Sciences, No. 19, Yu-quan Road, Beijing 100049, China
*Corresponding author: jingl@ciomp.ac.cn

Received 12 April 2017; revised 16 May 2017; accepted 16 May 2017; posted 17 May 2017 (Doc. ID 292760); published 7 June 2017

In order to meet the requirements of uniform illumination for optical palm/fingerprint instruments and overcome the shortcomings of the poor uniform illumination on the working plane of the optical palm/fingerprint prism, a novel secondary optical lens with a free-form surface, compact structure, and high uniformity is presented in this paper. The design of the secondary optical lens is based on emission properties of the near-infrared light-emitting diode (LED) and basic principles of non-imaging optics, especially considering the impact of the thickness of the prism in the design. Through the numerical solution of Snell's law in geometric optics, we obtain the profile of the free-form surface of the lens. Using the optical software TracePro, we trace and simulate the illumination system. The results show that the uniformity is 89.8% on the working plane of the prism, and the test results show that the actual uniformity reaches 85.7% in the experiment, which provides an effective way for realizing a highly uniform illumination system with high-power near-infrared LED.

OCIS codes: (080.4295) Nonimaging optical systems; (220.0220) Optical design and fabrication; (220.2945) Illumination design; (080.4225) Nonspherical lens design.

https://doi.org/10.1364/AO.56.004961

1. INTRODUCTION

Palm/fingerprint instruments are biometric identification equipment based on human biological characteristics, including ten fingerprints, rolling plane fingerprints, palm print, and side palm print. With the rapid popularization of safety monitoring systems in today's society, palm/fingerprint instruments have been widely adopted by government agencies and enterprise companies [1]. Palm/fingerprint identification can be classified into optical types, semiconductor types, and biological radio frequency (RF) types [2]. For the design of the illumination systems of the optical palm/fingerprint identification instruments [3,4], one of the key technical points is the working table with a high illumination uniformity. Light-emitting diodes (LEDs) are not only lightweight and have a long lifetime, but also consume less power [5,6]. Such advantages are very suitable for the illumination system of palm/fingerprint instruments, especially the directional emitting characteristics of the LED source, which makes the LED lighting system an easier way to realize uniform illumination.

Important in the lighting design of the LED source is how to improve the luminous efficiency and make the output beam meet the desired photometric specification. This is also applicable to palm/fingerprint illumination systems. Thus, it is necessary to add and optimize the optical structure of the secondary optic, so as to minimize the loss of the energy in the system and make the top plane of the palm/fingerprint prism meet uniform illumination requirements.

In order to overcome the shortcomings of the poor uniform illumination on the working plane of an optical palm/fingerprint prism, in this paper, a novel secondary optical lens with a free-form surface, compact structure, and high uniformity is presented. Optical performance of the novel secondary optical lens is investigated by both numerical simulation based on an optical software ray-tracing method and experiments. Results demonstrate that the novel secondary optical illumination system has better illumination uniformity performance of 85.7%, which is significantly higher than that of the normal design at 73% [7]. The novel design can meet the requirements of palm/fingerprint instruments well.

2. DESIGN METHOD

Optical palm/fingerprint identification has been used for a long time all over the world. The principle is to sense the ridges and valleys of a palm/finger through the total internal reflection (TIR). As shown in Fig. 1, in order to intuitively describe the working principle of the palm/fingerprint identification, the ridges and valleys structures of the palm/fingerprint only are shown and a partial amplification is made. Light from a source is incident to the bottom surface of the prism. The rays hit the top surface of the prism and then are split in two beams. One beam is totally internally reflected where the valleys of the palm/finger are located. However, the other beam is absorbed by the ridges of the palm/finger. The total internal reflected light is finally passed through the imaging optical system to a charge coupled device (CCD), so that the bright and dark palm/fingerprint image is obtained on the CCD. The amount of reflected light depends on the depth of the ridges and valleys, and the grease and water between the skin and the prism.

If one wants to get a high-quality palm/fingerprint feature image for easier data analysis, it is necessary that the plane of the prism has high illumination uniformity. In this paper, we adopt a high-power near-infrared LED as the light source, and add a secondary optical lens with a free-form surface structure in the illumination system. The uniform illumination effect on the glass plane of the prism can be realized.

The design of the secondary optical lens with realization of uniform illumination is based on the energy grid division, Snell's law, etc., in non-imaging optics [8,9]. At present, given the emission characteristics of an LED source, it is not difficult to achieve a circular uniform spot in the desired target surface by using these methods [10–12]. But in the optical palm/fingerprint instrument, the secondary optical lens designed according to the conventional method is no longer able to obtain a good illumination uniformity due to the presence of a prism with an excessive thickness (see the prism in Fig. 1). Thus, in this paper, we consider the impact of the thickness of the prism in the design step as described in the following.

A. Mapping Relationship from Source to Target

As shown in Fig. 2, the near-infrared LED source is located at the bottom of the palm/fingerprint instrument and the glass prism with a large thickness is in the middle, the upper and lower plane of which are parallel. The upper plane of the prism is regarded as the palm/fingerprint collection surface, i.e., the target surface of the illumination design. The first step of the novel secondary optical lens design in the palm/fingerprint

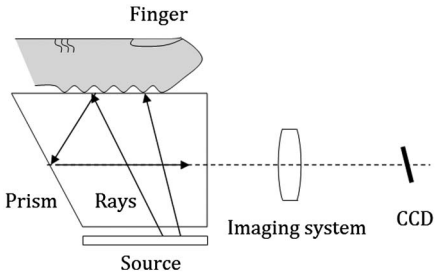

Fig. 1. Schematic of the optical system in a palm/fingerprint instrument.

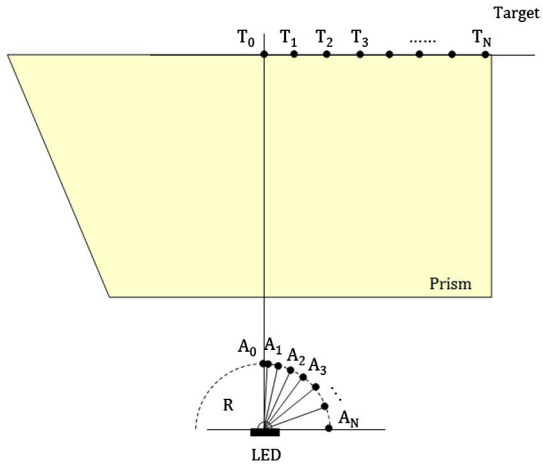

Fig. 2. Schematic of light energy mapping between the light source and target.

illumination system is to establish the energy mapping relationship from the LED source to the target plane [12]. In this design method, energy distribution of the LED source and illumination target plane are divided into several grids with equal optical power and area. Since both the source and target plane have axial symmetry, only one-quarter of the whole source and target plane are to be considered in this discussion (see Fig. 2). First, the energy distribution of the LED source is divided into N grids with equal optical power. A_1 to A_N at the bottom surface of the secondary optical lens correspond to the equal energy grids. The optical power of Ω_i can be expressed as follows:

$$\Phi_i = \iint I(\theta)\mathrm{d}\Omega_i, \tag{1}$$

where $I(\theta)$ is the light intensity distribution function, Ω_i is the i-th solid angle, and θ is the angle between the ray and the optical axis. Because the spatial light intensity of the high-power near-infrared LED used here is similar to Lambertian distribution, the equal angle θ_i with respect to equal division of energy can be calculated as

$$\theta_i = \sin^{-1}\sqrt{\frac{i}{N}}, \qquad i = 1, 2, 3, \ldots, N. \tag{2}$$

Second, because equal energy in equal area is equal illumination, an equal area division of the target plane is relatively easily gained without considering the light Fresnel loss and absorption loss. It can be divided into spaces T_1 to T_N as

$$T_i = \sqrt{\frac{i}{N}}T_N, \qquad i = 1, 2, 3, \ldots, N. \tag{3}$$

B. Construction of Secondary Optical Lens

As shown in Fig. 3, the aim of this design is to achieve uniform illumination of the target plane, that is, to make the equal energy edge rays ray_1 to ray_N emitted from the LED source arrive at the target plane points T_1 to T_N. The lower surface of the secondary optical lens is a designated surface, which is selected as a simple sphere. The center of the sphere is on the optical axis; it can be the origin of the LED source O, or not. When the center of the sphere is on the origin of the LED source, the

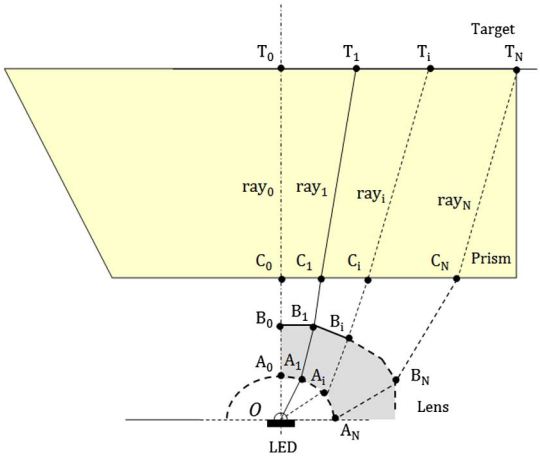

Fig. 3. Schematic of the ray trace in a uniform lighting system.

curvature of the sphere is not dependent on the thickness of the prism. However, once the center of the sphere is not on the origin of the LED source (on the optical axis), the curvature of the sphere is proportional to the thickness of the prism.

We consider the upper surface of the secondary optical lens as the unknown free-form surface that changes the optical path. The numerical solution of discrete points B_1 to B_N on the free-form surface is as follows.

As shown in Fig. 4(a), the height and central thickness of the secondary optical lens are h_1, t_1, respectively, so that the coordinates of A_0 and B_0 are $A_0(0, h_1)$, $B_0(0, h_1 + t_1)$, respectively. In Fig. 4(b), the total height of the illumination system is h_2, and the thickness of the prism is t_2. The coordinates of C_0 and T_0 can be obtained as $C_0(0, h_2 - t_2)$, $T_0(0, h_2)$, respectively. It is assumed that point B_i is on the tangent of its previous point B_{i-1}. Then the two objectives are to calculate the coordinate and tangent of B_i. For example, the first ray, ray_1, hitting at point A_1 on the lower surface of the secondary optical lens will exit from the lens at point B_1. Using tangent $\vec{T}_{B_0}$ of B_0 and refractive ray $\vec{A_1B_1}$ of ray_1, we can directly calculate the horizontal ordinate of B_1. The key point of the problem is to solve the tangent of B_1. By the Snell's law, knowing the incident ray $\vec{A_1B_1}$ and the refractive index of material, if one wants to calculate the tangent at B_1, the refractive ray $\vec{B_1C_1}$ must be obtained; namely, point C_1 must be calculated first.

Figure 4(b) shows that the first ray, ray_1, exiting from B_1 hits C_1 and then will be refracted into the prism. With the preknown point B_1 on the incident ray and T_1 on the refractive ray, Snell's law and the geometric relationship at point C_1 can be expressed as

$$\sin(\theta_{C_1}) = n \sin(\theta_{T_1}) \tag{4}$$

$$(C_{1z} - B_{1z}) \tan(\theta_{C_1}) + t_2 \tan(\theta_{T_1}) = T_{1y} - B_{1y}, \tag{5}$$

where θ_{C_1} and θ_{T_1} are the incident angle and refractive angle at point C_1, respectively. n is the refractive index of the prism, the optical axis is the z axis, and horizontal axis is the y axis. Combining Eqs. (4) and (5), we can get the incident angle

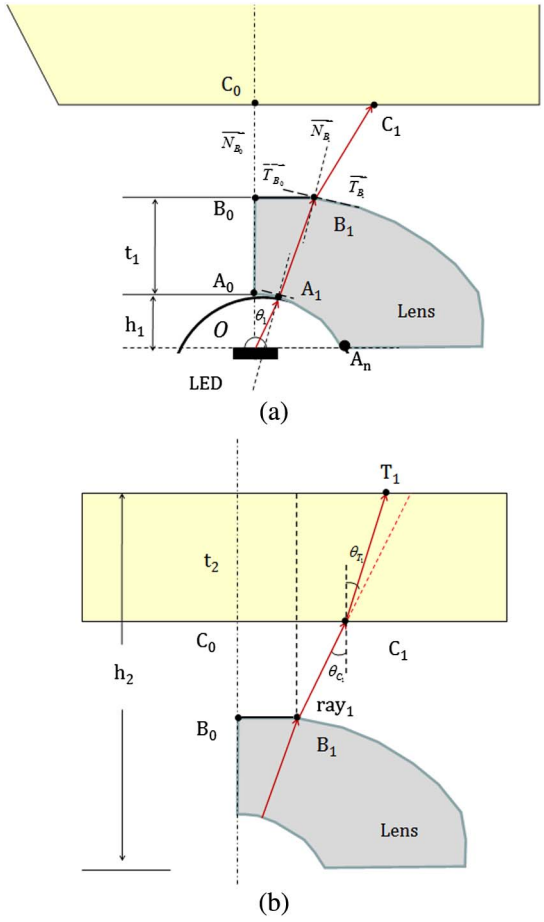

Fig. 4. (a) Schematic of ray_1's ray trace in the secondary optical lens. (b) Determination of the point C_1 on the lower surface of the prism.

θ_{C_1} and refractive angle θ_{T_1}, and then find the horizontal ordinate of C_1.

As shown in Fig. 5, the exiting ray $\vec{B_1C_1}$ has been deduced at point B_1. The tangent line $\vec{T}_{B_1}$ can also be obtained by Snell's law. The intersection of the tangent $\vec{T}_{B_1}$ and second ray, ray_2, is the second point B_2; its tangent solution process is similar to the solution of B_1. Likewise, the discrete sequence

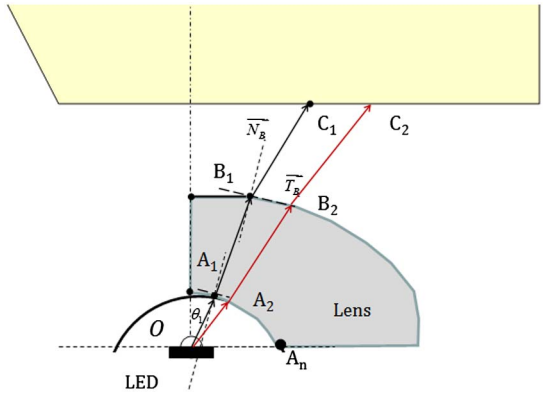

Fig. 5. Determination of the third point B_2 on the free-form surface of the secondary optical lens.

points B_3 to B_N can be obtained in this way. Finally, the free-form surface design process of the secondary optical lens has been completed. The profile of the free-form surface is fitted with these discrete points.

3. SIMULATION AND EXPERIMENTAL RESULTS

A. Simulation of High-Power Near-Infrared LED

Owing to the simulation reliability of the entire lighting system depending on the accuracy of the LED light source simulation, the optical model for a high-power near-infrared LED is built first. In this part, an Osram near-infrared LED of SFH 4235 [13] is simulated, which typically gives 950 mW optical power at 1 A at the wavelength of 850 nm. Figure 6 shows the structure of the LED provided by Osram and the optical model simulated in the TracePro software.

Figures 7(a) and 7(b) show the distribution curve of light intensity given by the technical manual of the near-infrared LED and the simulated distribution curve traced by two million rays in TracePro, respectively. The normalized cross correlation (NCC) [14] is the quantitative value for evaluating the approximation of two curves, which is written as Eq. (6):

$$\mathrm{NCC} = \frac{\sum_x \sum_y (A_{xy} - \overline{A})(B_{xy} - \overline{B})}{\sqrt{\sum_x \sum_y (A_{xy} - \overline{A})^2 \sum_x \sum_y (B_{xy} - \overline{B})^2}}, \tag{6}$$

where A_{xy} and B_{xy} are the intensity or irradiance of the manufactures (A) and the simulation values (B), respectively. $\overline{A}(\overline{B})$ is the mean value of the $A(B)$ across the x–y plane.

The higher the NCC value, the more approximate the two curves. Apparently the simulation result is in good agreement with the given distribution curve. The normalized NCC value of the two curves is up to 99.2%, which verifies the accuracy of this optical modeling.

B. Simulation of Illumination System

In this section, a specific secondary optical design example is given to verify the accuracy of the above method. The bottom sphere of the secondary optical lens has a radius of 4 mm and central thickness of 4 mm, and the lens is made of polycarbonate (PC) material with a refractive index of 1.58 at a wavelength of 850 nm. The glass prism is made of K9 material with a refractive index of 1.51 at a wavelength of 850 nm, and the corresponding thickness and lighting area are 83 mm and 130 mm × 130 mm, respectively. The LED is 6 mm away from the bottom of the secondary lens. The number of rays N is 100, and more rays can be used. The more rays used, the higher the precision of the lens surface. In this paper, we used $N = 100$ rays to calculate the free-form surface of the lens, which is enough for the processing level at present. The discrete points of the free-form surface, namely, B_0 to

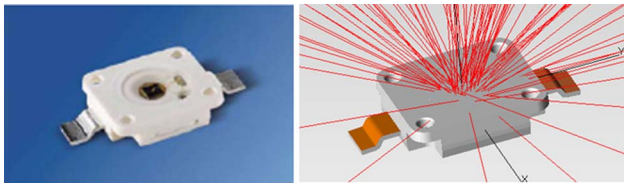

Fig. 6. 3D modeling and ray tracing of the near-infrared LED.

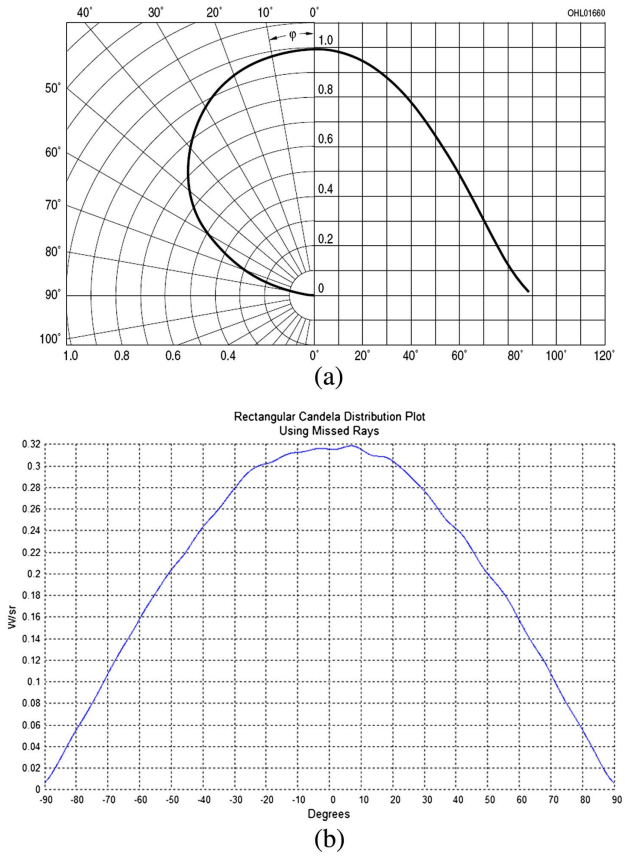

Fig. 7. (a) Candela distribution of the near-infrared LED provided by the manufacturer. (b) Rectangular candela distribution of the near-infrared LED in TracePro.

B_N, are successively obtained by the designing process described in part 2. In Fig. 8(a), the blue circle points represent the discrete points and the curve is the fitting data by the 10th-order polynomial. The residual error of the fitting is also shown in Fig. 8(b). The error gives a maximum of 0.017 mm, which meets the accuracy requirement for processing.

Using the Scheme language embedded in TracePro, the 3D model of the secondary optical lens can be acquired by rotating the obtained curve against the symmetrical axis. Considering the actually required illumination of the palm/fingerprint, three predesigned lenses are arranged in triangle, as shown in Fig. 9.

The ray tracing and the analysis of the illumination system are thereby conducted. Figure 10 shows the ray tracing by Monte Carlo in TracePro, and we can see that most of the LED rays are incident to the top plane of the prism in the palm/fingerprint illumination system.

Figure 11 shows the simulation results of the irradiation on the glass plane of the prism, which gives a good uniformity of lighting. The corresponding value of uniformity (U) can be obtained in Eq. (7),

$$U = 1 - \varepsilon = \left(1 - \sqrt{\frac{\sum_{i=1}^{M} (E_i - \overline{E})^2}{M\overline{E}^2}}\right) \times 100\%, \tag{7}$$

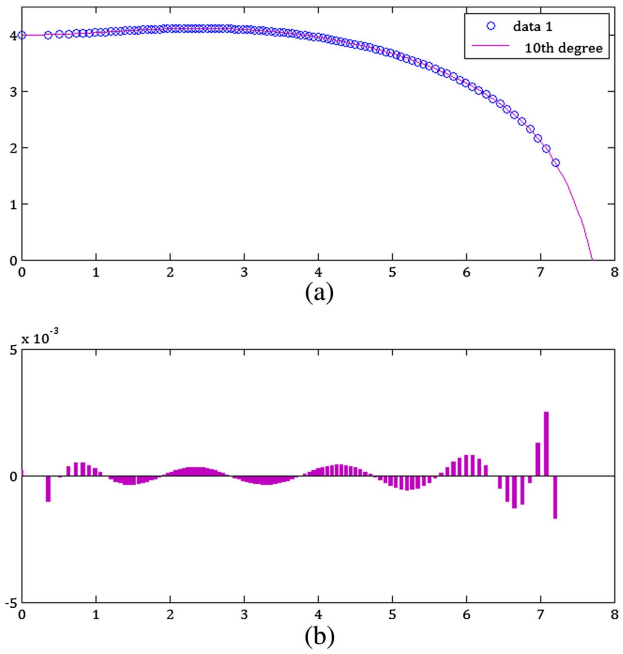

Fig. 8. (a) Profile of the free-form surface of the secondary optical lens with 10th-degree polynomial fitting. (b) The residuals of the 10th-degree polynomial fitting.

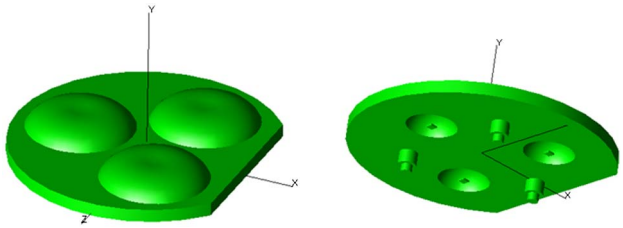

Fig. 9. 3D modeling of the secondary optical lens array in TracePro.

where M is the number of sampling points, E_i is the corresponding irradiance of each point, and $\overline{E}$ is the averaged irradiance.

The area of the glass plane of the prism is divided into 7×7 grids of equal area. The number of the equal area grids can be more, which depends on the test accuracy requirements. Table 1 shows the irradiance (W/m^2) of 49 sampling points. According to Eq. (7), the U is obtained to be 89.8%.

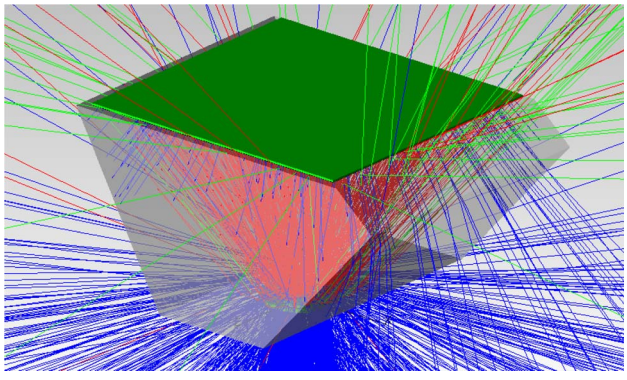

Fig. 10. Ray tracing of the palm/fingerprint lighting system.

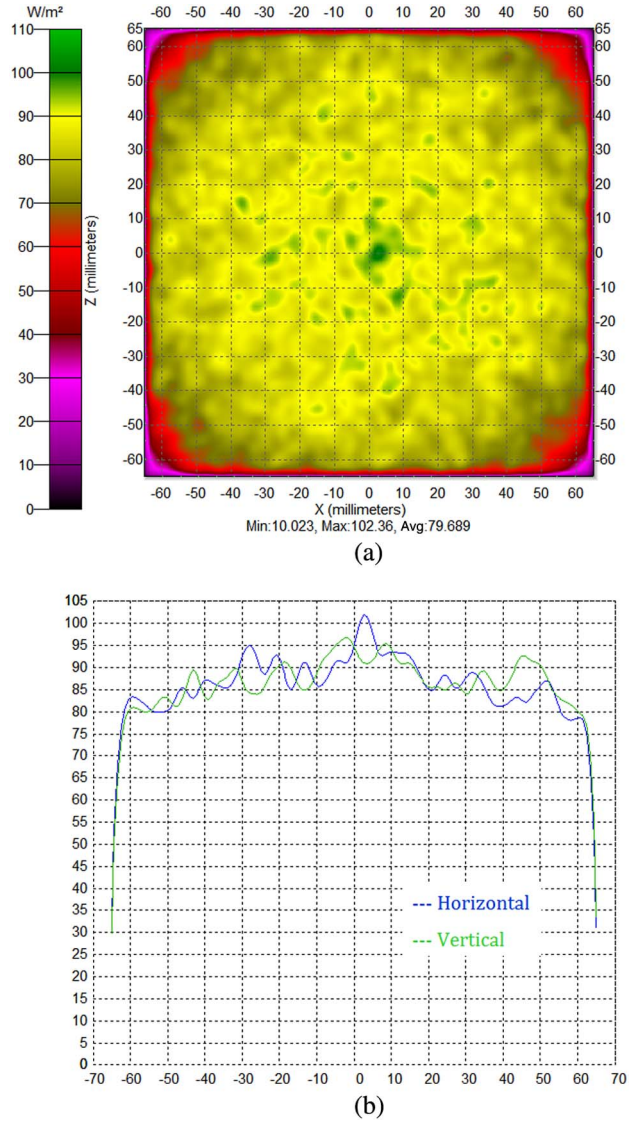

Fig. 11. (a) Irradiance map on the top plane of the prism in the palm/fingerprint lighting system. (b) Profiles of the irradiance map on the top plane of the prism in the palm/fingerprint lighting system.

Table 1. Simulated Irradiance Map on Plane of Prism Divided by 7 × 7 Sampling Points

	1	2	3	4	5	6	7
1	58.4	75.1	80.4	84.2	80.1	75.5	58.0
2	74.9	83.2	85.6	85.5	86.0	82.9	76.2
3	81.8	86.6	87.0	87.4	87.2	86.7	79.6
4	81.2	86.3	89.2	91.6	88.0	86.5	81.0
5	81.5	86.7	87.6	88.5	87.9	87.4	81.6
6	73.5	82.5	86.5	87.7	84.6	83.6	74.9
7	57.3	74.0	80.4	81.5	80.2	73.9	57.5

C. Experiment of the Illumination System

In this work, the designed secondary optical lens is made of PC, which can be easily injection-molded. The left part in Fig. 12 shows the processed optical lens, and the right part in Fig. 12 shows the lens fixed on the circuit board by pins. Figure 13 shows the completed palm/fingerprint instrument and photograph of the top plane of the prism. With the proposed design method, a good irradiance uniformity is achieved. For analyzing the uniformity in application, the area of the glass plane of the prism is also divided into a 7×7 grid, and the irradiance (W/m^2) is measured by the laser power meter of NOVA II of the Ophir company. Table 2 shows the measured irradiance of 49 sampling points. Because of the actual lens processing, packaging, assembling, test equipment, and other errors, energy loss is introduced, which makes the actual values in Table 2 significantly lower than those in Table 1 on the whole. As a result, the U is calculated to be 85.7%, which is slightly lower than the theoretical value of 89.8%. The difference is mainly also derived from optical modeling, lens processing and packaging, test equipment, and other errors.

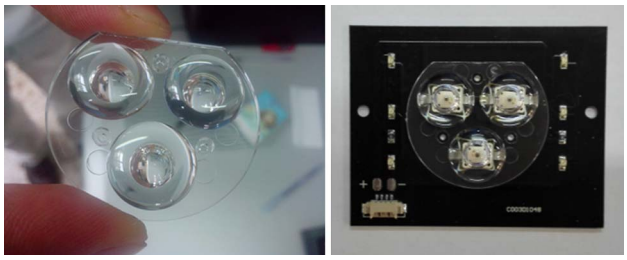

Fig. 12. Completed palm/fingerprint lighting system with near-infrared LED and secondary lens array.

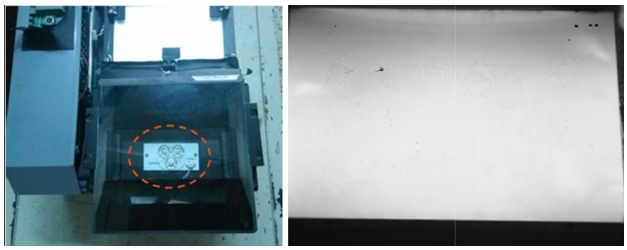

Fig. 13. Completed palm/fingerprint instrument and photograph of the top plane of the prism.

Table 2. Test Irradiance Map on Plane of Prism Divided by 7 × 7 Sampling Points

	1	2	3	4	5	6	7
1	42.5	43.2	49.7	53.6	51.6	45.5	41.8
2	49.2	53.9	59.7	64.2	55.2	51.2	47.3
3	56.1	58.8	64.7	66.4	63.0	57.1	53.7
4	57.2	62.1	68.7	70.1	67.6	61.8	58.6
5	53.1	55.9	63.2	67.9	62.3	57.6	55.4
6	46.6	48.8	55.6	58.9	56.8	53.1	47.1
7	41.3	45.0	47.8	53.0	47.4	44.2	43.2

The processing, assemblage, and testing of the palm/fingerprint illumination system with a high-power near-infrared LED is introduced in this paper, and a good irradiance uniformity is achieved that can effectively avoid the irradiance being too high at the center and being too low on the edge. As a result, the over-saturated brightness at the center and the insufficient brightness on the edge can be removed in the follow-up image processing.

4. CONCLUSION

To meet the uniformity requirement in palm/fingerprint identification, a compact secondary optical lens is designed for the high-power near-infrared LED based on the theory of Snell's law and non-imaging optics. Using the optical software TracePro, we trace and simulate the designed system. The processing, assemblage, and testing of the palm/fingerprint illumination system is also conducted in this work. The simulation results and measured results are both of a satisfactory uniformity higher than 85%.

Funding. 863 Program (2015AA03A101); National Major Instrument Project (2013YQ140517).

REFERENCES

1. X. Liu, F. Zaki, Y. Wang, Q. Huang, X. Mei, and J. Wang, "Secure fingerprint identification based on structural and microangiographic optical coherence tomography," Appl. Opt. **56**, 2255–2258 (2017).
2. S.-W. Back, Y.-G. Lee, S.-S. Lee, and F.-S. Son, "Moisture-insensitive optical fingerprint scanner based on polarization resolved in-finger scattered light," Opt. Express **24**, 19195–19202 (2016).
3. W. Huang, "Optical design of high performance fingerprint scanner with large capture size," Chin. Opt. Lett. **10**, 122201 (2012).
4. S. M. Rao, "Method for producing correct fingerprints," Appl. Opt. **47**, 25–29 (2008).
5. F. M. Steranka, J. Bhat, D. Collins, L. Cook, M. G. Craford, R. Fletcher, N. Gradner, P. Grillot, W. Goetz, M. Keuper, R. Khare, A. Kim, M. Krames, G. Harbers, M. Ludowise, P. S. Martin, M. Misra, G. Mueller, R. Mueller-Mach, S. Rudaz, Y.-C. Shen, D. Steigerwald, S. Stockman, S. Subramanya, T. Trottier, and J. J. Wierer, "High power LEDs technology status and market applications," Phys. Status Solidi A **194**, 380–388 (2002).
6. D. G. Pelka and K. Patel, "An overview of LED applications for general illumination," Proc. SPIE **3781**, 15–26 (2003).
7. J. Y. Joo, D.-K. Woo, S. S. Park, and S.-K. Lee, "Design and fabrication of a fingerprint imager with compact LED illumination and compact imaging optics," Opt. Express **18**, 18932–18944 (2010).
8. M. Bass, E. W. Van Stryland, D. R. Williams, and W. L. Wolfe, *Handbook of Optics*, 2nd ed. (Optical Society of America, 1995), pp. 1.12–1.14.
9. W. Roland, M. Juan, and B. Pablo, *Nonimaging Optics* (Elsevier Academic, 2004).
10. F. Chen, S. Liu, K. Wang, Z. Liu, and X. Luo, "Free-form lenses for high illumination quality light-emitting diode MR16 lamps," Opt. Eng. **48**, 123002 (2009).
11. Z. Zhenrong, H. Xiang, and L. Xu, "Freeform surface lens for LED uniform illumination," Appl. Opt. **48**, 6627–6634 (2009).
12. G. Wang, L. Wang, L. Li, D. Wang, and Y. Zhang, "Secondary optical lens designed in the method of source-target mapping," Appl. Opt. **50**, 4031–4036 (2011).
13. http://www.osram.com.
14. C. C. Sun, T. X. Lee, S.-H. Ma, Y.-L. Lee, and S.-M. Huang, "Precise optical modeling for LED lighting verified by cross correlation in mid-field region," Opt. Lett. **31**, 2193–2195 (2006).